Macromolecules

ARTICLE

pubs.acs.org/Macromolecules

Salient Features in Uniaxial Extension of Polymer Melts and Solutions: Progressive Loss of Entanglements, Yielding, Non-Gaussian Stretching, and Rupture

Yangyang Wang and Shi-Qing Wang*

Department of Polymer Science, University of Akron, Akron, Ohio 44325, United States

ABSTRACT: The nonlinear responses of an entangled SBR melt and its solutions in rapid uniaxial extension have been studied by rheometric and rheo-optical measurements. During (startup) extension, the samples progressively lose entanglements. At relatively low rates, all entanglements are eventually lost, leading to yielding, nonuniform extension, and ductile specimen failure. At sufficiently high rates, some entanglements survive to allow non-Gaussian stretching and full chain extension leading to rupture-type sample breakdown when the failure mechanism switches from disentanglement, i.e., mutual chain sliding, to chain scission. The precursor to rupture, i.e., non-Gaussian stretching, is evidenced by the birefringence measurements that show the breakdown of the linear stress−optical relation. The corresponding critical stress is found to be proportional to the polymer concentration, in agreement with a scaling analysis based on an entanglement network picture. The onset of non-Gaussian stretching and rupture occurs at higher stretching ratios when the entanglement strands are made longer by dilution as achieved in the three solutions. In other words, both yielding and rupture occur at higher strains with increasing entanglement spacing, underscoring the legitimacy to represent entangled polymers in terms of an elastic network when depicting their predominant nonlinear responses to rapid uniaxial extension.

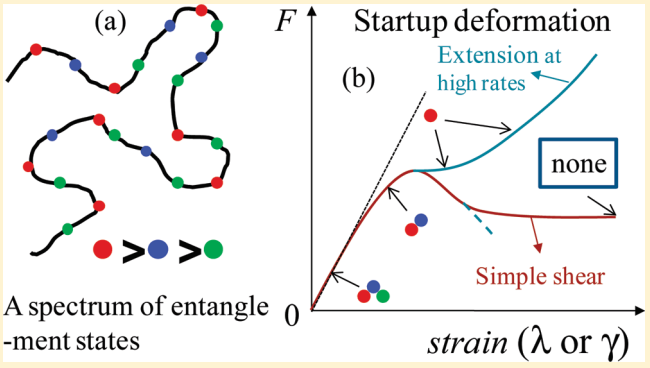

1. INTRODUCTION

Polymer entanglement is a crucial concept in the description of chain dynamics and rheology of polymeric liquids. Because of chain entanglement, concentrated polymer solutions and melts of high molecular weight display a number of unique features such as elastic strain recovery, plateau in stress relaxation, and dynamic shear measurements as well as the familiar 3.4 power law scaling of the zero-shear viscosity with molecular weight.[1,2] The first attempt to depict the entanglement phenomenon came from Green and Tobolsky,[3] Yamamoto,[4] and Lodge,[5] who extended the classical theory of rubber elasticity[6−10] to polymeric liquids, i.e., entangled melts and solutions, by considering a temporary network with constantly breaking and re-forming local junctions. During the past three decades, the study of the dynamics of entangled polymers has been dominated by the application of the tube-reptation theory that evolved from the reptation idea of de Gennes[11] to a systematic theoretical formulation of polymer dynamics by Doi and Edwards.[12−16]

The entanglement spacing M_e, defined as the average molecular weight between neighboring entanglements in a melt, is an important structural parameter in both transient network models and the tube-reptation theory. The end-to-end distance between entanglements l_{ent} is related to M_e as $l_{ent} = l_K(N_e)^{1/2}$, i.e., $(l_{ent})^2 \sim M_e$, where $N_e = M_e/m_K$, with m_K being the mass corresponding to one Kuhn length l_K and is given in terms of the molar mass per backbone bond m_1 as $m_K = m_1(C_\infty + 1)^2/C_\infty$.[17] When a pure melt is swollen by a solvent, the entanglement spacing associated with the solute polymer increases. Extensive experimental and theoretical studies[18−21] have revealed that in theta solvents or concentrated solutions the entanglement spacing scales with the concentration as $M_e(\phi) = M_e\phi^{-1.3}$.

The subchains between entanglements are typically assumed to exhibit the ideal Gaussian chain behavior. However, at large deformations where the limiting extensibility of the entanglement strands is approached, the subchains are expected to become non-Gaussian, leading to breakdown of the linear stress−optical relation (SOR).[22−27] A recent experimental study on uniaxial extensional deformation of a styrene−butadiene random copolymer (SBR) melt has confirmed a yield-to-rupture transition,[28] when a sufficiently high rate of extension causes the melt to approach the finite extensibility limit where a sharp rise in the tensile force due to strong non-Gaussian stretching resulted in rupture-like failures in the so-called "glass-like" zone.[29]

Despite the continuous reference to the idea of representing polymeric liquids of high molecular weight as an entanglement network in the past half a century, the concept of entanglement spacing in the network picture rarely appeared explicitly in any experimental description of nonlinear rheological responses. If

Received: February 23, 2011
Revised: May 2, 2011
Published: June 09, 2011

Table 1. Molecular Characteristics of the Long-Chain and Short-Chain SBR Melts

sample	M_n (kg/mol)	M_w/M_n	η_0 (kPa·s)	styrene (%)	butadiene (%)	1,2-BD (%)
SBR1M	1068	1.23		22	78	29
SBR20K	20		2.2			

an entangled polymer could really be represented as a Gaussian chain network, a finite chain extensibility limit might appear in experiment. Few experimental studies systematically probed this limit apart from several reports on simultaneous measurements of mechanical stress and optical birefringence in entangled polymers undergoing rapid uniaxial extension.[22,26,27]

In the network picture of entangled polymers, any non-Gaussian response would be due to excessive chain stretching between entanglements. An entangled polymeric liquid with greater entanglement spacing should be more stretchable before exhibiting the non-Gaussian behavior. In this work, we vary the range of entanglement spacing by examining a set of samples made of a pure melt of high molecular weight and several of its blends with a short-chain component that can be treated as entangled solutions. We aim to determine whether the onset of non-Gaussian stretching and rupture-like failure would scale with the polymer concentration ϕ (that dictates the entanglement spacing) in a predictable manner.

Specifically, we have carried out rapid uniaxial extension experiments on a series of a SBR melt and its solutions, where the weight fraction ϕ ranges from 1.0 to 0.4. The onset of non-Gaussian stretching has been identified by both mechanical and optical measurements. Our experiments lead to the following conclusions: (a) the critical stress for the stress−optical relation (SOR) failure is proportional to ϕ in agreement with a network-picture-based prediction; (b) strong non-Gaussian stretching appears at sufficiently high rates when the failure mechanism switches from yield to rupture; (c) the critical stretching ratios for non-Gaussian stretching as well as rupture increase with the entanglement spacing; (d) entanglements dissolve progressively and sequentially during startup deformation to allow stretching well beyond the affine condition, under which the strands between the equilibrium entanglement points would be straightened at a stretching ratio around 4.

2. EXPERIMENTAL SECTION

2.1. Materials. Three concentrated solutions were prepared from a long-chain (1M) and a short-chain (20K) styrene−butadiene random copolymer (SBR) synthesized by anionic polymerization at Bridgestone Americas Center for Research and Technology via courtesy of Xiaorong Wang. The molecular characteristics of these long-chain and short-chain SBR melts are listed in Table 1. The solutions were prepared at the long-chain's weight fractions equal to 80%, 60%, and 40%, by first dissolving both the long-chain and short-chain SBR melts in toluene and subsequently removing the solvent under vacuum.

The linear viscoelastic properties of the pure SBR1M melt and concentrated solutions were first evaluated by performing small-amplitude oscillatory shear measurements on an ARES-LS rheometer at different temperatures with 8 mm diameter parallel plates. Figure 1 shows the master curves at room temperature (23−25 °C) of the frequency dependence of storage and loss moduli for the 1M/20K solutions, constructed by using the time−temperature superposition principle.[30] The equilibrium plateau modulus $G_{eq}(\phi)$, the number of entanglements

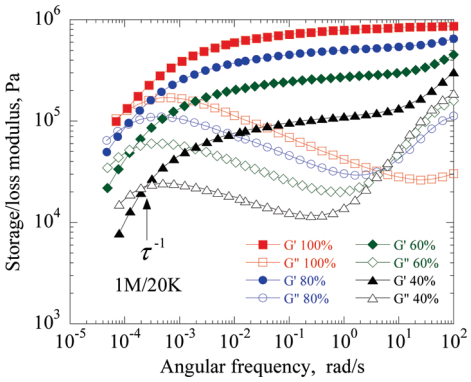

Figure 1. Small-amplitude oscillatory shear measurements of the pure SBR1M and its 1M/20K binary mixtures at room temperature. The indicated concentrations represent the weight fractions of the long chains in the blends. The storage and loss moduli are plotted as a function of angular frequency in filled and open symbols, respectively.

Table 2. Linear Viscoelastic Properties of the Melt and Solutions

sample	$G_{eq}(\phi)$ (MPa)	Z	M_e (kg/mol)	$\tau(\phi)$ (s)	$\tau_R(\phi)$ (s)	$\tau_R'(\phi)$ (s)
1M	0.85	510	2.6	11000	7.2	5.7
1M (80%)	0.51	380	3.5	9700	8.5	7.6
1M (60%)	0.27	270	4.9	7100	8.8	9.0
1M (40%)	0.10	150	8.8	4100	9.1	12

per chain Z, the terminal relaxation time $\tau(\phi)$, and Rouse relaxation time $\tau_R(\phi)$ for the melt and solutions have been calculated and listed in Table 2. The equilibrium plateau modulus $G_{eq}(\phi)$ is taken from the value of storage modulus G' at the frequency where the loss modulus G'' shows a minimum. The terminal relaxation time $\tau(\phi)$ is calculated as the reciprocal of the crossover frequency ω_c where $G' = G''$. The SBR20K has a terminal relaxation time of ∼7 ms at room temperature (23−25 °C), which is significantly lower than that of any of the three solutions shown in Table 2. Therefore, the short chains can be considered as "solvent" in the binary mixtures, whose contributions to the plateau modulus $G_{eq}(\phi)$ and tensile force are negligible compared to those of the long chains at the experimentally explored frequency and rate ranges in this study. The equilibrium plateau modulus $G_{eq}(\phi)$ is found to scale with the concentration ϕ as $G_{eq}(\phi) \sim \phi^{2.3}$, in agreement with previous studies in the literature.[18−21] There are two different approaches in the literature to evaluate the Rouse relaxation time, and these can lead to somewhat different values.[31−34] In the present work, the Rouse relaxation times of the pure melt and its solutions are conveniently estimated from the reptation time $\tau(\phi)$ as $\tau_R(\phi) = \tau(\phi)/3Z(\phi)$ as prescribed by a generalization of the Doi−Edwards tube model.[20] An alternative way to estimate τ_R ensures[35] that it scales with molecular weight quadratically but yields similar values as shown in Table 2 in the symbol of τ_R'.

The specimens for the extensional tests were prepared by first pressing the SBR1M melt and its solutions into a thin film between two Teflon plates in a CARVER hydraulic press at 60 °C. To obtain smooth surfaces, the samples for the rheo-optical measurements were then further molded between two pieces of cover glass with CARVER under slight pressure at the same temperature. The samples were allowed to relax for a period of at least 12 h at room temperature, before being removed from the Teflon and glass surface with the aid of dry ice. The final rectangular sheet-like specimens were cut out from the thin

dx.doi.org/10.1021/ma200432q |Macromolecules 2011, 44, 5427–5435

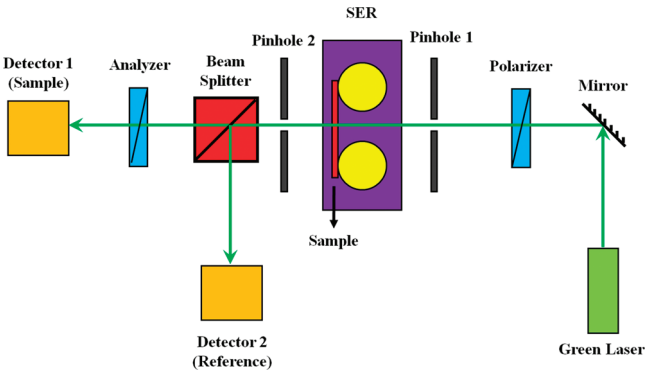

Figure 2. Schematic drawing of the rheo-optical setup for simultaneous measurements of extensional stress and optical birefringence, resembling the design of Venerus and co-workers.[22,27]

film by a razor blade. The typical dimension of the sample was 25 mm × 5 mm × 0.5 mm.

2.2. Apparatus. *2.2.1. Extensional Fixture.* Most of the uniaxial extension experiments were carried out using a first generation SER fixture[36,37] mounted on an ARES-LS rotational rheometer, except for the ones on the SBR1M melt, which were performed on a Physica MCR 301 rheometer. The SER fixture modified the fiber wind-up design of Macosko and co-workers,[38,39] in which the length of the stretching zone remained a constant during extension. A constant Hencky strain rate therefore could be easily obtained on this fixture by applying a constant angular velocity to turn the two drums, on which the sample is wrapped around. To achieve better friction between the sample and the drums that are held tight by clamps, a piece of sandpaper (120 grit aluminum oxide, Virginia Abrasives) was glued to the surface of each drum.

2.2.2. Birefringence Setup. Polymers typically exhibit linear proportionality between stress σ and birefringence Δn, i.e., $\Delta n = C\sigma$ in uniaxial extension where C is the stress−optical coefficient.[40] The validity of such a stress−optical rule (SOR) has been used to justify the tube model evaluation of shear stress based on only intrachain elastic retraction. When the network chain becomes non-Gaussian, the SOR breaks down. Thus, birefringence measurements can provide important and independent characterization of any non-Gaussian responses. The flow birefringence setup shown in Figure 2 adopts the design of previous workers.[22,27] In each measurement, a linearly polarized green laser (λ = 532 nm) was split into two beams after passing through the stretched sample on the SER fixture. One of the beams was used as the reference beam, and the other passed through the analyzer and read by the "sample" detector. The sample retardance δ during stretching can be related to the voltage readings of the two detectors by

$$\frac{V_{\text{sample}}}{V_{\text{ref}}} = A \sin^2\left(\frac{\delta}{2}\right) \quad (1)$$

where V_{sample} and V_{ref} are the voltages measured by the sample and reference detector, respectively, and A is a constant close to unity, which was calibrated before each experiment by changing the orientation of the analyzer. The absolute birefringence $|\Delta n|$ can be calculated from δ according to

$$|\Delta n| = \frac{\delta\lambda}{2\pi d} \quad (2)$$

where λ is the wavelength of the laser source and d is the sample thickness at each moment of stretching. We note that we were not able to conduct birefringence measurements beyond Hencky strain of ∼2, where the clamps of SER would start to block the optical path.

3. RESULTS

3.1. Yielding and Rupture in Startup Extension. Two distinct types of responses were observed for the SBR1M melt and its solutions during rapid uniaxial extension at a constant strain rate. In Figure 3a−d, the engineering stress σ_{engr} (proportional to the total tensile force) is shown as a function of the stretching ratio, along with the stress−strain curve from the classical rubber elasticity theory,[6−10] also known in the rheology community as the neo-Hookean model, for the four samples, involving the equilibrium plateau moduli listed in Table 2: $\sigma_{\text{engr}} = G_{\text{eq}}(\lambda - 1/\lambda^2)$. At low rates, the sample became nonuniform shortly after reaching an engineering stress maximum. These experiments are plotted in Figure 3a−d in the open symbols.

At sufficiently high rates, sharp rupture occurred when the engineering stress increases monotonically, displaying a marked upturn as shown by the filled symbols. The two representative photographs in Figure 4a,b show the difference between necking and rupture, taken during and after constant rate stretching of the 80% solution at 0.1 and 6.0 s^{-1}, respectively. In Figure 4a, the dashed line defines the stretching zone on the SER fixture. The necking such as shown by the photo in Figure 4a was progressive and persisted until the sample eventually broke apart. The nonuniform extension, i.e., necking, involves irrecoverable deformation or flow since the sample could not restore its original dimensions. In contrast, when rupture is the mode of failure, the sample after breakup could return to its original dimensions, as shown in Figure 4b.

It is worth noting that the nonuniform stretching or necking takes place at rather high Weissenberg number $Wi = \dot{\varepsilon}\tau \gg 1$, where $\dot{\varepsilon}$ denotes the Hencky strain rate. In this regime, the surface tension has a negligible effect on the extensional behavior of the highly elastic entangled melts.

3.2. Failure of Linear Stress−Optical Relation. Apart from the appearances of failure, there are a couple of other features to distinguish yielding from rupture. At low rates when yielding occurs as evidenced by the pronounced maximum of the engineering stress,[41] we observe the stress−optical relationship to be linear. At sufficiently high extensional rates Figure 5a−d shows the absolute optical birefringence $|\Delta n|$ as a function of the true stress σ during uniform extension for the SBR melt and solutions. For each sample, the data collected at different rates fall onto a unique curve, indicating that the linear stress−optical relationship (SOR) holds up to a critical stress independent of the applied rate, with the coefficient C being the same for all the samples. The straight line with slope 1.0 in each of Figure 5a−d represents a linear stress−optical relationship. A departure from the SOR is observed beyond a critical stress level, where the true stress grows faster than the optical birefringence. The dashed vertical lines in Figure 5 indicate the onset of the SOR failure for each sample. It is clear from Figure 5 that the critical stress $\sigma^*(\phi)$ decreases with lower polymer concentration ϕ. It remains to be discussed below about how $\sigma^*(\phi)$ should decrease with ϕ according to a basic scaling analysis.

4. DATA ANALYSES AND DISCUSSION

4.1. Onset of Non-Gaussian Stretching. There are more than one indications of non-Gaussian stretching leading to rupture at sufficiently high rates. The upturn of the engineering stress in Figures 3a−d is one signature, preceded by the strain softening that is due to partial yielding arising from some level of

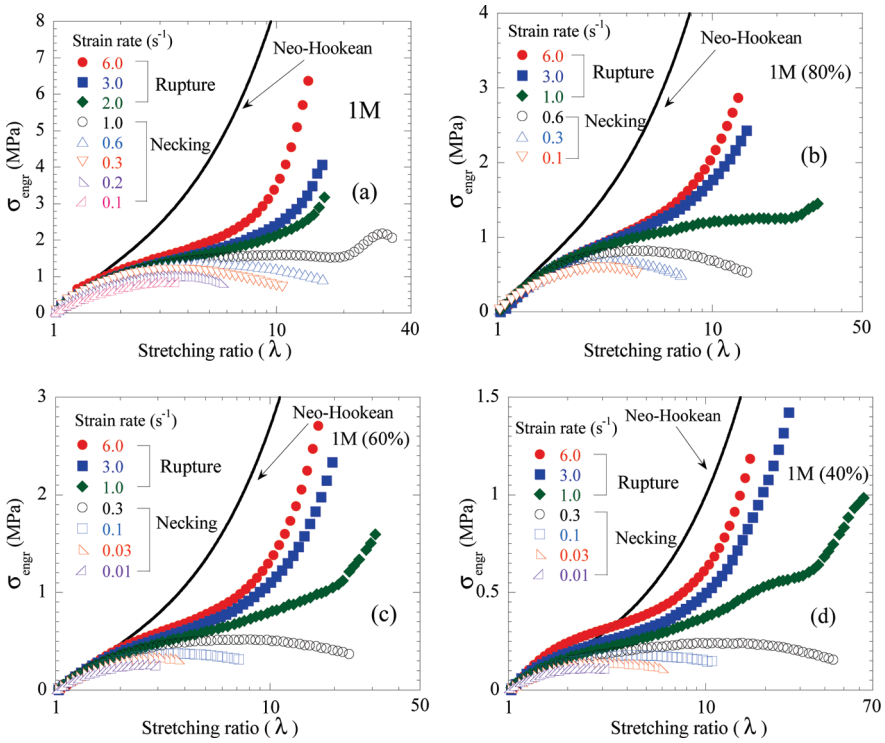

Figure 3. Engineering stress σ_{engr} vs stretching ratio λ curves for (a) SBR1M melt and (b) 1M (80%), (c) 1M (60%), and (d) 1M (40%) solutions at various strain rates. The continuous line denotes the calculation from the classical rubber elasticity theory (neo-Hookean model). The open and filled symbols represent the stretching that ends up in necking (nonuniform extension) and rupture, respectively. In the case of necking, the end of each stress−strain curve represents the onset of nonuniform extension by visual inspection.

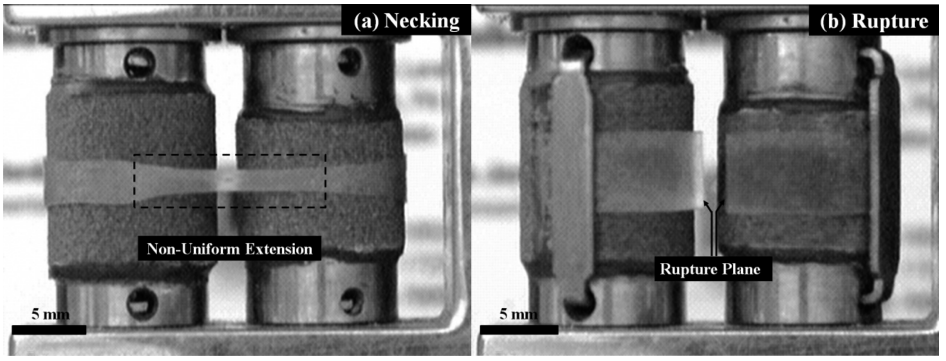

Figure 4. (a) Photograph taken during the extension of 1M (80%) solution at Hencky strain rate 0.1 s^{-1}. The sample suffered nonuniform extension, i.e., necking, at high strains, as shown in the rectangular region defined by the dashed line. (b) Photograph taken after rupture during the extension of 1M (80%) solution at strain rate 6.0 s^{-1}. The sample ruptures by forming a sharp crack, and the broken parts snapped back and returned to their original dimensions.

chain mutual sliding[42] up to a point when the surviving entanglement points lock in to produce strain hardening due to non-Gaussian stretching.

The non-Gaussian stretching can be characterized in a more insightful way. Consider the classical rubber elasticity theory, i.e., the neo-Hookean model: $\sigma_{engr} = G_{eff}(\lambda - 1/\lambda^2)$, where G_{eff} is an effective plateau modulus and λ is the stretching ratio. If we regard the deviation of the data in Figure 3a−d from the neo-Hookean curve as due to partial yielding or loss of chain entanglement during extension, the subsequent upturn may be analyzed with a neo-Hookean relation involving a softer network. In other words, some chain entanglements are missing due to the ongoing chain stretching that produces the force imbalance.[42] As a consequence, the network effectively becomes softer with a lower elastic modulus. Namely, the system has an effective G_{eff} that varies with λ and applied rate. Figure 6a,b shows for two samples that at these sufficiently high rates the samples stop losing chain entanglement before the point of rupture. This calibration of the stress−stretching data against the neo-Hookean model actually serves two purposes: (a) providing evidence for non-Gaussian stretching of the surviving entanglement network; (b) identifying how much entanglement loss has occurred. At these high rates, the occurrence of non-Gaussian stretching suggests that at the remaining entanglements the interchain topological interactions

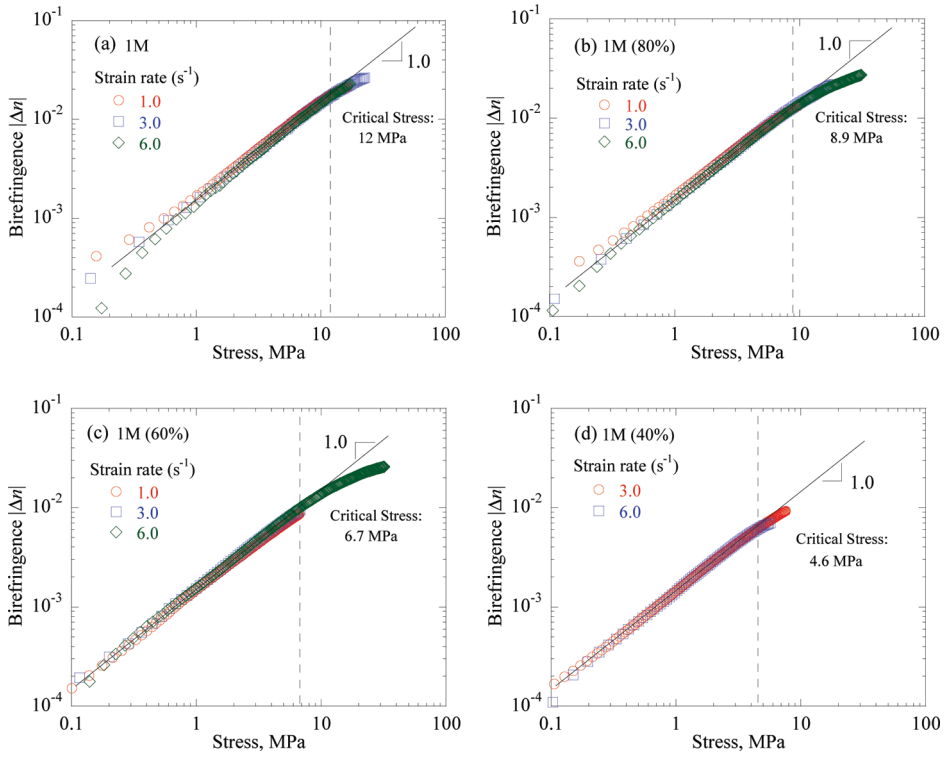

Figure 5. Absolute birefringence $|\Delta n|$ as a function of true stress for (a) SBR1M pure melt and (b) 1M (80%), (c) 1M (60%), and (d) 1M (40%) solutions. The onset of stress−optical relation failure is marked by the dashed vertical line. The stress−optical coefficient C appears to be concentration independent, as expected, equal to 1.5×10^{-3} MPa^{-1} for the SBR1M melt and its concentrated solutions.

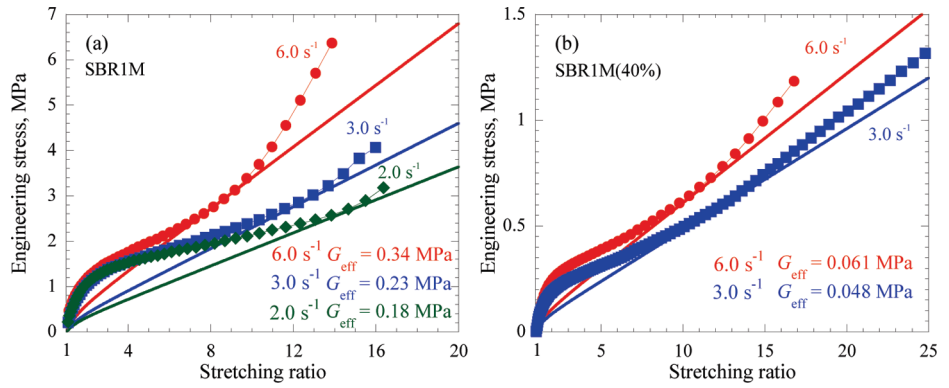

Figure 6. Engineering stress σ_{engr} versus the stretching ratio λ for (a) SBR1M and SBR1M (40%). The solid curves represent the neo-Hookean model with a reduced effective modulus G_{eff}.

are so strong that force imbalance[42] does not occur and chain stretching can approach the finite chain extensibility limit. It is also clear from Figure 6a,b that as the applied Hencky rate decreases few entanglement points survive as shown by the reduced effective plateau modulus G_{eff}.

4.2. Full Extension of Entanglement Strands and Concentration Dependence. Previous studies[22−27] have already suggested that the departure from the stress−optical relation (SOR) at high stresses, as shown in Figure 5a−d, is a result of the non-Gaussian stretching. It is necessary to analyze the critical condition for the breakdown of SOR as a function of the polymer concentration ϕ. We find, by reading the critical stresses from Figure 5a−d, that the onset stress for the SOR failure scales linearly with ϕ as shown in Figure 7. The following analysis indicates that the scaling behavior of the critical stress and corresponding degree of extension can be understood in terms of finite chain extensibility and non-Gaussian chain stretching of the surviving entanglement network.

At any given stage during fast extension that produces macroscopic rupture, the stretched specimen may be modeled as a transient Gaussian chain network with an effective plateau modulus $G_{eff}(\phi)$ and entanglement spacing $l_{eff\text{-}ent}(\phi)$ that can be longer than the equilibrium entanglement spacing of $l_{ent}(\phi)$. For extensions with a sufficiently high Hencky rate so that some entanglements may be regarded as permanent, the stress−strain relationship may be approximated by the classical rubber

dx.doi.org/10.1021/ma200432q |Macromolecules 2011, 44, 5427–5435

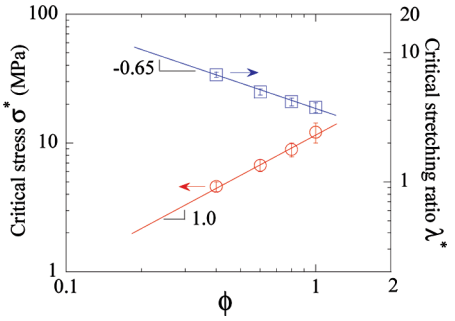

Figure 7. Concentration ϕ dependence of the critical stress σ^* and critical stretching ratio λ^* at the onset of the stress−optical relation (SOR) failure in the binary mixtures of SBR1M and SBR20K. The critical stresses are the ones identified earlier in Figure 5. They appear to be insensitive to the applied rates. The critical stretching ratio λ^* is calculated from eq 3, with the critical stress σ^* and plateau modulus G_{eff} as inputs.

elasticity theory as[6−10]

$$\sigma(\phi) = G_{eff}(\phi)\left[\lambda^2(\phi) - \frac{1}{\lambda(\phi)}\right] \simeq G_{eff}(\phi)\lambda^2(\phi) \quad (3)$$

where $G_{eff}(\phi)$ is related to the average end-to-end distance of the load bearing strand between the effective entanglements, $l_{eff\text{-}ent}(\phi)$, as

$$G_{eff}(\phi) \sim \frac{\phi}{l^2_{eff\text{-}ent}(\phi)} \sim \frac{\phi}{M_{eff\text{-}e}(\phi)} \quad (4)$$

with $M_{eff\text{-}e}(\phi)$ being the molecular weight of the strand.

In absence of a rigorous theory, we assume that eqs 3 and 4 hold up to the onset of non-Gaussian stretching. When non-Gaussian stretching is approached, the end-to-end distance of the entanglement strand would approach $l_K N_{eff\text{-}e}(\phi)$, corresponding to an onset stretching ratio $\lambda^*(\phi)$ given by

$$\lambda^*(\phi) \sim \frac{l_K N_{eff\text{-}e}(\phi)}{l_K\sqrt{N_{eff\text{-}e}(\phi)}} = \sqrt{N_{eff\text{-}e}(\phi)} = \frac{l_{eff\text{-}ent}(\phi)}{l_K} \quad (5)$$

Insertion of eqs 4 and 5 into eq 3 produces

$$\sigma^*(\phi) \simeq \frac{\phi}{l^2_{eff\text{-}ent}(\phi)}\left[\frac{l_{eff\text{-}ent}(\phi)}{l_K}\right]^2 \sim \phi \quad (6)$$

Thus, the concentration dependence expressed by eq 6 is consistent with the scaling behavior observed experimentally in Figure 7. In other words, another way to examine the validity of eqs 3 and 5 is to plot the critical stretching ratio $\lambda^*(\phi) \sim [\sigma^*(\phi)/G_{eff}(\phi)]^{1/2}$ as a function of ϕ as shown Figure 8. Since $l_{eff\text{-}ent}(\phi) \sim [G_{eff}(\phi)/\phi]^{1/2} \sim \phi^{1.3/2}$, the revealed scaling exponent of 0.65 for λ^* is not accidental and is consistent with eqs 3 and 5.

We note that the demonstration of $\sigma^* \sim \phi$ is based on the validity of eqs 3 and 4, which are a description of Gaussian chain network by the neo-Hookean model. It is not difficult to realize that $\sigma^* \sim \phi$ should be truly independent of any specific model because the strength of the network with polymer fraction ϕ at rupture should indeed scale with the concentration ϕ.

4.3. Progressive Loss of Entanglement during Deformation. We can actually estimate the value λ^* of eq 5, under the idealized condition that all equilibrium chain entanglements survive during extension, by determining the equilibrium entanglement

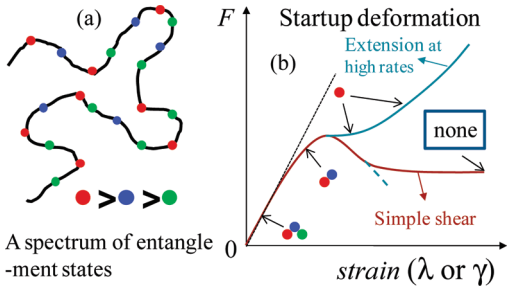

Figure 8. (a) Schematic depiction of chain entanglement distribution in a test chain in terms of the entanglement strength. The red dots represent the strongest chain entanglements whereas the green ones represent the weakest. (b) All entanglements from the red to green are present in equilibrium. Upon startup deformation of extension or shear, the force response vs strain is as depicted where the corresponding states of entanglement are indicated. The curve with an upturn corresponds to extension to non-Gaussian stretching and rupture whereas the dashed line represents yielding leading to nonuniform extension. The progressive loss of chain entanglement in the form of mutual chain sliding first takes place at the weakest entanglement points. In the flow state of shear, none of the entanglements survive; i.e., all parts of a chain slide past its surrounding chains at all times.

Table 3. Characteristic Parameters of PBD and PS

polymer	l_{ent} (Å) (ref 45)	l (Å) (ref 46)	C_∞ (refs 45 and 46)	$\lambda_{eq}{}^*$
1,4-PBD	41.7	1.47	5.5−5.6	4.3−4.4
PS	76.5	1.54	9.6−10	4.1−4.5

spacing l_{ent} and the Kuhn length l_K associated with pure 1, 4-polybutadiene and polystyrene, respectively, using[17,43] either $l_K = l(C_\infty + 1)$ or $l_K = C_\infty l/\cos(\theta/2)$ with the bond angle[44] $\theta = 68°$. Table 3 lists the calculated values of $\lambda_{eq}{}^* = l_{ent}/l_K$ for both PB and PS. Although we do not have direct experimental data of l_{ent} and l_K of the SBR melt, we can expect a similar value of $\lambda_{eq}{}^* \sim 4$ for the SBR melt.

The strands between entanglements would be fully straightened at a stretching ratio of $\lambda_{eq}{}^* \sim 4$ if the affine deformation would prevail. We would expect the tension within the load bearing strands to build up to the point of chain scission leading to the macroscopic specimen rupture. But this apparently does not happen in extension of non-cross-linked melts. In other words, the specimen does not rupture at the stretching ratio $\lambda_{eq}{}^* \sim 4$ at all. Actually, the specimen would not rupture until a stretching ratio λ as high as 14 according to Figure 6a. Thus, a significant fraction of entanglements that exist in equilibrium clearly did not survive during extension. Upon losing sufficient entanglements due to the force imbalance,[42] there will be fewer entanglements per chain so that $l_{eff\text{-}ent}$ between the surviving entanglement points could be much longer than l_{ent}.

Since the shear modulus G_{eff} in eq 3 is proportional to the number density of the surviving (load bearing) entanglement strands, any loss of chain entanglement during extension should produce a reduction in G_{eff} from the equilibrium plateau modulus G_{eq}. Figure 6a shows the effective modulus G_{eff} at different applied rates, which is considerably lower than $G_{eq} = 0.85$ MPa. This partial loss of entanglements indicates that not all entanglements are equally strong; i.e., there is a strength spectrum of

dx.doi.org/10.1021/ma200432q |Macromolecules 2011, 44, 5427–5435

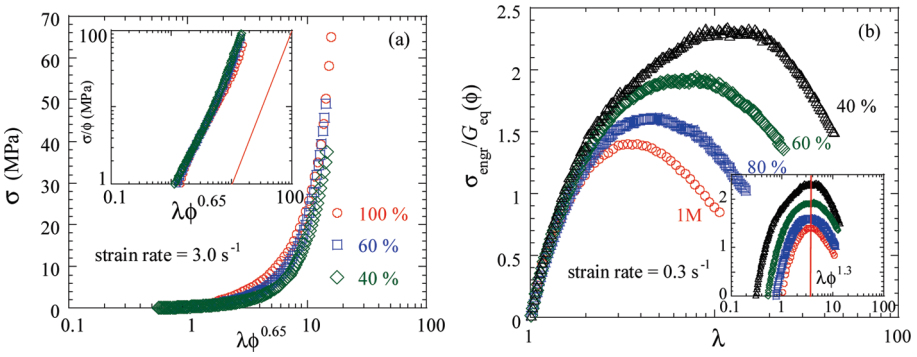

Figure 9. (a) True stress vs normalized stretching ratio $\lambda\phi^{0.65}$ curves for the SBR1M and its solutions at a strain rate of 3.0 s^{-1}. The inset shows the normalized true stress σ/ϕ as a function of the normalized stretching ratio $\lambda\phi^{0.65}$ or $\lambda/\lambda^*(\phi)$ with $\lambda^*(\phi) \sim l_{ent}(\phi) \sim \phi^{-0.65}$. (b) Normalized engineering stress vs stretching ratio curves for the SBR1M melt and its solutions at strain rate 0.3 s^{-1}. The normalized engineering stress σ_{engr} is defined as the ratio of engineering stress σ_{engr} to the equilibrium plateau modulus G_{eq}. The inset shows that the stretching ratio at the maximum tensile force, λ_{max}, appears to scale linearly with $M_e(\phi) \sim [l_{ent}(\phi)]^2 \sim \phi^{-1.3}$.

intermolecular interactions along any given test chain. Thus, any test chain may be depicted as shown in Figure 8 where we designate chain entanglements of three different strengths for illustration purposes. The force imbalance occurs[42] first for some entanglement strands formed at the weakest (green) entanglement points where mutual chain sliding takes place first. Whenever and wherever the chain sliding occurs, the corresponding "entanglement" point may be regarded as lost. By statistical ensemble average, stronger entanglement points may still exist uniformly along the linear chain as shown by the red dots in Figure 8. When only the strongest entanglements are present, the total entanglements per chain drop from 20 to 8 in the schematic representation of Figure 8. Conversely, the molecular weight $M_{eff\text{-}e}$ between entanglements becomes 2.5 times equilibrium entanglement molecular weight M_e, leading to the reduction in the effective plateau modulus from G_{eq} to $G_{eff} = 0.4G_{eq}$. This picture explains, even at a sufficiently high rate of 6 s^{-1} for the pure SBR1M in Figure 6a, how an entangled polymer first undergoes partial "yielding" and loses some entanglements and then undergoes non-Gaussian stretching thanks to the remaining strong entanglement points until the point of rupture.

In this picture, we can crudely describe the effect of Hencky rate as follows. At lower rates, only a smaller fraction of entanglements survive, leading to a looser entanglement network with entanglement spacing $l_{eff\text{-}ent} > l_{ent}$ and consequently more reduced plateau modulus $G_{eff} \sim 1/(l_{eff\text{-}ent})^2$ according to eq 4. On the other hand, the non-Gaussian stretching occurs at a higher stretching ratio of $\lambda^* \sim l_{eff\text{-}ent}$ according to eq 5, so that the Cauchy stress σ^* at the onset of non-Gaussian stretching would remain constant: As shown in eq 6, σ^* is independent of $l_{eff\text{-}ent}$ and therefore the applied rate. This conclusion is consistent with the findings in Figure 5a−d. This invariance allows us to estimate the onset extensional stress σ^* in the limit of no entanglement loss so that we can use the equilibrium values G_{eq} and $\lambda_{eq}{}^*$ in eq 3 to find $\sigma^* \sim 0.85 \times 4^2 = 13.6$ MPa, in the case of the pure SBR1M melt. This value is surprisingly close to the experimentally observed value of ca. 12 MPa in Figure 5a. It is worth noting that according to Luap and co-workers[22] polystyrene melts have a critical stress of 2.7 MPa, which yields a critical stretching ratio of 3.7 from $\lambda_{eq}{}^* = (\sigma^*/G_{eq})^{1/2}$ of eq 3 based on the plateau modulus of polystyrene[45] $G_{eq} = 0.2$ MPa. This value of $\lambda_{eq}{}^*$ is fairly close to that listed in Table 3.

Loss of chain entanglements occurs progressively during extension, and only the strongest entanglements survive at high rates, leading to rupture instead of necking. The concept of a spectrum of entanglement strength as depicted in Figure 8 makes it plausible to explain why the preceding estimate of full chain extension of equilibrium entanglement strands at $\lambda_{eq}{}^* \sim 4$ is a good indication of when nonaffine deformation takes place and why the sample actually ruptures at significantly higher stretching ratios. For example, referring to Figure 7a, the rupture of the 1M pure SBR at 6 s^{-1} occurs at $\lambda_{rupture} \sim 14$, which is 3.5 times $\lambda_{eq}{}^* \sim 4$. This would imply, given $(M_{eff\text{-}e})^{1/2} \sim l_{eff\text{-}ent} \sim \lambda_{rupture}$ according to eq 5, at the point of rupture the molecular weight between the remaining entanglements has increased by a factor of $M_{eff\text{-}e}/M_e = (\lambda_{rupture}/\lambda_{eq}{}^*)^2 = (3.5)^2 \sim 12$; i.e., only 1 out of 12 equilibrium entanglements survived. Conversely, we have arrived at an interesting plausible conclusion. If an entangled polymer has only 12 entanglements per chain, it would never be able to produce a stretching ratio of 14 to experience rupture. In other words, at temperatures well above the glass transition temperature, weakly entangled polymers may not undergo chain scission no matter what rate is applied.

4.4. Extensibility of Solutions with Greater Entanglement Spacing. Upon swelling of the entanglement network to enlarge the entanglement spacing in solutions the onset of non-Gaussian stretching and corresponding rupture should occur at higher stretching ratios. Figure 7 clearly points to this trend. Figure 9a indeed shows at a high extensional rate of 3.0 s^{-1} that the stress versus extension curves exhibit an upturn at the same value of the normalized stretching ratio, i.e., $\lambda/\lambda_{eq}{}^*(\phi)$ or $\lambda\phi^{0.65}$, where $\lambda_{eq}{}^* \sim l_{ent}(\phi) = l_{ent}(\phi = 1)\phi^{-0.65}$. The inset of Figure 9a shows that after the initial transients the stress σ would rise with the stretching ratio λ quadratically, in apparent agreement with the neo-Hookean behavior for a network with a fixed number density of load-bearing strands. This coincidence occurs as a combination of progressive loss of entanglement and non-Gaussian stretching. If the non-Gaussian stretching yielding a stronger than quadratic dependence on λ, i.e., $\sigma = G_{eff}\lambda^q$ (where $q > 2$) and meanwhile the loss of chain entanglement leads to $M_e(\lambda) \sim \lambda^p$ or $G_{eff} \sim \lambda^{-p}$, then the two exponents are related as $q = 2 + p$ to produce the apparent scaling of $\sigma \sim \lambda^2$ as shown in the inset of Figure 9a.

It is even more interesting to compare the degrees of extension at the engineering stress maxima as a function of polymer

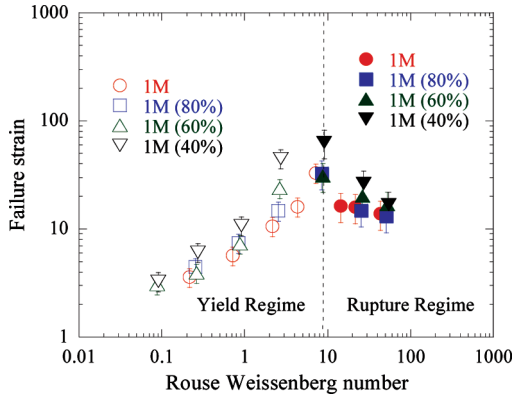

Figure 10. Strains at failure as a function of the Rouse Weissenberg number. The applied rates are 6.0, 3.0, 2.0, 1.0, 0.6, 0.3, 0.2, and 0.1 s^{-1} for the SBR1M melt; 6.0, 3.0, 1.0, 0.6, 0.3, and 1.0 s^{-1} for the 80% solution; 6.0, 3.0, 1.0, 0.3, 0.1, 0.03, and 0.01 s^{-1} for the 60% solution; 6.0, 3.0, 1.0, 0.3, 0.1, 0.03, and 0.01 s^{-1} for the 40% solution. The Rouse Weissenberg number is the strain rate times the Rouse relaxation time listed in Table 2. The failure strain corresponds to the last point of each stress−strain curve where nonuniform stretching or rupture occurs. The open and filled symbols represent the stretching that ends up either necking or rupture. The vertical line indicates the critical Rouse Weissenberg number at the yield-to-rupture transition, which is about 9 for all the solutions and melt.

concentration. In our previous investigations,[41,42] we proposed that the global yielding in a startup rapid uniaxial extension at the tensile force peak is the consequence of imbalance between intermolecular gripping force and intrachain elastic retraction force. Specifically, the intermolecular gripping force may increase with the applied rate and decrease with increasing chain deformation. Since the strands between entanglements are longer for the solutions, higher stretching ratios can be accessed without reaching the finite extensibility limit. Consequently, the decline of the interchain molecular gripping force[42] is a weaker function of the stretching ratio. In other words, the imbalance between intermolecular gripping force and retraction force may occur at larger stretching ratios at a lower concentration. The second factor leading to even higher stretching ratios at the point of the tensile force maximum is that chain retraction force should build up more slowly in solutions since the longer strands reach the finite extensibility limit at a higher stretching ratio.

The data Figure 9b can be explained precisely in this manner: solutions with a lower concentration exhibit higher yield strain and normalized yield stress. Since the Rouse times τ_R of these four samples are comparable, the common rate of 0.3 s^{-1} corresponds to the same Rouse Weissenberg number, i.e., the product of τ_R and strain rate. The tensile force indeed peaks at a significantly higher stretching ratio $\lambda \sim 10$ in the 40% solution than in the pure SBR1M melt ($\lambda \sim 3$). Actually, the stretching ratio at the maximum tensile force, λ_{max} appears to scale linearly with $M_e(\phi) \sim [l_{ent}(\phi)]^2 \sim \phi^{-1.3}$ so that $\lambda\phi^{1.3}$ causes the peak positions of the three curves to line up as shown in the inset of Figure 9b, in contrast to the onset of upturn in Figure 9a that collapse when plotted $\lambda/l_{ent}(\phi) \sim \lambda\phi^{0.65}$. These differences are clearly discernible and must be taken seriously. They reflect how the different physics dictate the yielding behavior and the onset of non-Gaussian stretching, respectively.

4.5. Yield-to-Rupture Transition. Figure 10 summarizes the trends found in Figure 9a,b. More importantly, the critical rate for the yield-to-rupture transition appears to be the same. Since all four samples have comparable Rouse relaxation time τ_R, the critical condition for rupture actually corresponds to a critical Rouse Weissenberg number $Wi_{Rouse} = \dot{\varepsilon}\tau_R$, where $\dot{\varepsilon}$ denotes the extensional strain rate. Apparently, for the chains to avoid yielding, the extensional rate needs to be sufficiently high relative to the rate at which the polymer chains execute Rouse motions.

The rupture is likely due to chain scission when strong non-Gaussian stretching has built up sufficient tension within the entanglement strands.[28,47] Currently, we do not have any direct experimental proof of chain scission though the rupture is in every way identical to rupture seen in cross-linked SBR. Moreover, according to the analysis given in the ending paragraph of subsection 4.3, at the point of rupture, there still survive 510/12 ∼ 42 entanglements per chain. In other words, it is implausible for the stretched specimen to run out of entanglement at a stretching ratio of 14. When the applied rate becomes sufficiently low, all the entanglements can escape due to force imbalance,[42] and the entanglement strands can no longer reach the finite extensibility limit. Non-Gaussian chain stretching does not occur, and the failure mode switches from the rupture mode to the yielding mode where chains mutually slide past one another instead of suffering chain scission. This transition is rheologically evident from Figure 3a−d as the curves of engineering stress vs the stretching ratio switch from those of monotonic upturn to those with a clear maximum—the peak would have been sharper had the SBR1M melt been far more monodisperse. The contrast between yielding and rupture is evident from the rheometric data only when represented in terms of the tensile force. In comparison, the traditional expression of the mechanical responses in terms of the true stress would never show signature for the yield-to-rupture transition.

Figure 10 presents the critical strain for the sample failure as a function of the Rouse Weissenberg number. The critical strain for the onset of nonuniform stretching increases monotonically with increasing strain rate, as represented by the open symbols. The yield-to-rupture transition occurs around Rouse Weissenberg number around 9, consistent with our previous result.[28] In the rupture regime, the critical strain decreases with strain rate, as shown by the filled symbols. The rate dependence of the critical strain in the rupture regime is in agreement with the characterization of the "glass-like" zone by Malkin and Petrie.[29] The decrease of the critical (apparent) strain for rupture with increasing rate occurs as the experimental condition approaches closer to the affine deformation limit.

5. CONCLUSIONS

In summary, a well-entangled SBR melt undergoes a yield-to-rupture transition beyond a critical rate in rapid uniaxial extension. The transition is plausibly caused by a change of the failure mechanism from chain disentanglement (yielding) to chain scission. Rupture occurs when the strands between entanglements undergo non-Gaussian stretching on their path to full extension, where the linear stress−optical relation (SOR) breaks down. Detailed analysis of the nonlinear responses upon fast extension suggests that there is a spectrum of entanglement strength. The emerging picture is that the weaker entanglements with lower intermolecular gripping forces first disappear as a result of the force imbalance leading to mutual chain sliding, leaving only the stronger entanglements to hold up the cohesive integrity of the sample. In other words, entanglements disappear

progressively along any given chain in the sample as depicted in Figure 8. At low enough rates, even the strongest entanglements do not survive during continuing extension, and disentanglement, i.e., mutual chain sliding occurs. This yielding typically results in strain localization that is responsible for the specimen failure. However, at sufficiently high rates, the surviving entanglements allow the sample to access non-Gaussian chain stretching, approach the finite chain extensibility limit and eventually suffer rupture.

The characteristic nonlinear rheological behavior of the well-entangled solutions is similar to that of the well-entangled melt. For example, the three SBR solutions also experience yielding or non-Gaussian stretching and rupture-like failure in the explored range of extensional rates. We found the critical stress for non-Gaussian stretching is proportional to the polymer concentration consistent with the network picture. With decreasing polymer concentration, the strands between entanglements grow longer, leading to a more extendable network. As a consequence, yielding occurs at a higher stretching ratio, and rupture also occurs at a greater degree of extension, both relative to the behavior of the pure melt.

AUTHOR INFORMATION

Corresponding Author
*E-mail: swang@uakron.edu.

ACKNOWLEDGMENT

The authors express their sincere gratitude to Dr. Xiaorong Wang from Bridgestone-Americas Center for Research and Technology for providing the SBR samples in this study. This work is supported, in part, by a grant (DMR-0821697) and (CMMI-0926522) from the National Science Foundation.

REFERENCES

(1) Graessley, W. W. *Adv. Polym. Sci.* **1974**, *16*, 1.
(2) Lodge, T. P.; Rotstein, N. A.; Prager, S. *Adv. Chem. Phys.* **1990**, *79*, 1.
(3) Green, M. S.; Tobolsky, A. V. *J. Chem. Phys.* **1946**, *14*, 80.
(4) Yamamoto, M. *J. Phys. Soc. Jpn.* **1956**, *11*, 413.
(5) Lodge, A. S. *Trans. Faraday. Soc.* **1956**, *52*, 120.
(6) Guth, E.; James, H. M. *Ind. Eng. Chem.* **1941**, *33*, 624.
(7) James, H. M. *J. Chem. Phys.* **1943**, *11*, 455.
(8) Flory, P. J.; Rehner, J. *J. Chem. Phys.* **1943**, *11*, 512.
(9) Wall, F. T. *J. Chem. Phys.* **1942**, *10*, 132.
(10) Wall, F. T. *J. Chem. Phys.* **1943**, *11*, 527.
(11) de Gennes, P. G. *J. Chem. Phys.* **1971**, *55*, 572.
(12) Doi, M.; Edwards, S. F. *J. Chem. Soc., Faraday Trans. 2* **1978**, *74*, 1789.
(13) Doi, M.; Edwards, S. F. *J. Chem. Soc., Faraday Trans. 2* **1978**, *74*, 1802.
(14) Doi, M.; Edwards, S. F. *J. Chem. Soc., Faraday Trans. 2* **1978**, *74*, 1818.
(15) Doi, M.; Edwards, S. F. *J. Chem. Soc., Faraday Trans. 2* **1979**, *75*, 38.
(16) Doi, M.; Edwards, S. F. *The Theory of Polymer Dynamics*; Oxford University Press: Oxford, 1986.
(17) Wang, S. Q. *Macromolecules* **2007**, *40*, 8684.
(18) Colby, R. H.; Fetters, L. J.; Funk, W. G.; Graessley, W. W. *Macromolecules* **1991**, *24*, 3873.
(19) Colby, R. H.; Rubinstein, M. *Macromolecules* **1990**, *23*, 2753.
(20) Wang, S. F.; Wang, S. Q.; Halasa, A.; Hsu, W. L. *Macromolecules* **2003**, *36*, 5355.
(21) Yang, X.; Wang, S. Q.; Ishida, H. *Macromolecules* **1999**, *32*, 2638.
(22) Luap, C.; Müller, C.; Schweizer, T.; Venerus, D. C. *Rheol. Acta* **2005**, *45*, 83.
(23) Matsumoto, T.; Bogue, D. C. *J. Polym. Sci., Polym. Phys. Ed.* **1977**, *15*, 1663.
(24) Muller, R.; Froelich, D. *Polymer* **1985**, *26*, 1477.
(25) Muller, R.; Pesce, J. J. *Polymer* **1994**, *35*, 734.
(26) Rothstein, J. P.; McKinley, G. H. *J. Non-Newtonian Fluid Mech.* **2002**, *108*, 275.
(27) Venerus, D. C.; Zhu, S. H.; Öttinger, H. C. *J. Rheol.* **1999**, *43*, 795.
(28) Wang, Y. Y.; Wang, S. Q. *Rheol. Acta* **2010**, *49*, 1179.
(29) Malkin, A. Y.; Petrie, C. J. S. *J. Rheol.* **1997**, *41*, 1.
(30) Ferry, J. D. *Viscoelastic Properties of Polymers*, 3rd ed.; Wiley: New York, 1980.
(31) Menezes, E. V.; Graessley, W. W. *J. Polym. Sci., Polym. Phys. Ed.* **1982**, *20*, 1817.
(32) Osaki, K.; Nishizawa, K.; Kurata, M. *Macromolecules* **1982**, *15*, 1068.
(33) Osaki, K.; Uematsu, T.; Yamashita, Y. *J. Polym. Sci., Part B: Polym. Phys.* **2001**, *39*, 1704.
(34) Roland, C. M.; Archer, L. A.; Mott, P. H.; Sanchez-Reyes, J. *J. Rheol.* **2004**, *48*, 395.
(35) Osaki, K.; Nishizawa, K.; Kurata, M. *Macromolecules* **1982**, *15*, 1068–1071.
(36) Sentmanat, M. L. *Rheol. Acta* **2004**, *43*, 657.
(37) Sentmanat, M. L.; Wang, B. N.; McKinley, G. H. *J. Rheol.* **2005**, *49*, 585.
(38) Macosko, C. W.; Lornston, J. *Annu. Tech. Conf.-Soc. Plast. Eng.* **1973**, *19*, 461.
(39) Padmanabhan, M.; Kasehagen, L. J.; Macosko, C. W. *J. Rheol.* **1996**, *40*, 473.
(40) Janeschitz-Kriegl, H. *Polymer Melt Rheology and Flow Birefringence*; Springer: Berlin, 1983.
(41) Wang, Y. Y.; Wang, S. Q. *J. Rheol.* **2008**, *52*, 1275.
(42) Wang, Y. Y.; Wang, S. Q. *J. Rheol.* **2009**, *53*, 1389.
(43) Hiemenz, P. C.; Lodge, T. P. *Polymer Chemistry*; CRC Press: Boca Raton, FL, 2007.
(44) Rubinstein, M.; Colby, R. H. *Polymer Physics*; Oxford University Press: Oxford, 2003.
(45) Fetters, L. J.; Lohse, D. J.; Richter, D.; Witten, T. A.; Zirkel, A. *Macromolecules* **1994**, *27*, 4639.
(46) Aharoni, S. M. *Macromolecules* **1983**, *16*, 1722.
(47) Kamei, E.; Onogi, S. *Appl. Polym. Symp.* **1975**, *27*, 19.